ISSN 1063-7842, Technical Physics, 2006, Vol. 51, No. 1, pp. 112–117. © Pleiades Publishing, Inc., 2006.
Original Russian Text © A.K. Vershovskii, M.V. Balabas, A.É. Ivanov, V.N. Kulyasov, A.S. Pazgalev, E.B. Aleksandrov, 2006, published in Zhurnal Tekhnicheskoĭ Fiziki, 2006, Vol. 76, No. 1, pp. 115–120.

EXPERIMENTAL INSTRUMENTS AND TECHNIQUES

Fast Three-Component Magnetometer–Variometer Based on a Cesium Sensor

A. K. Vershovskii*, M. V. Balabas, A. É. Ivanov**, V. N. Kulyasov**, A. S. Pazgalev*, and E. B. Aleksandrov***

** Ioffe Physicotechnical Institute, Russian Academy of Sciences, Politekhnicheskaya ul. 26, St. Petersburg, 194021 Russia*
e-mail: antver@mail.ioffe.ru
*** Vavilov State Optical Institute, All-Russia Research Center, Birzhevaya liniya 12, St. Petersburg, 199034 Russia*
e-mail: balabas@soi.spb.ru

Received May 30, 2005

Abstract—A new fast three-component variometer–magnetometer based on a cesium sensor is developed and tested. The device is intended for measuring the longitudinal component of the geomagnetic field in the range from 20 to 65 μT and two transverse components in the range ±1 μT. The reproducibility of measurements is ±0.15 nT, and the noise-limited sensitivity is 0.01 nT (in terms of the rms deviation) or 0.04″ for a measurement time of 0.1 s.

PACS numbers: 85.70.Ay

DOI: 10.1134/S1063784206010166

1. STATEMENT OF THE PROBLEM

In this paper, we describe a vector magnetometer–variometer (VMV) intended for simultaneously measuring the variations of all three components of a magnetic field with a rate of up to ten measurements per second. The device is an implementation of the idea of a vector magnetometer based on a scalar sensor placed in a variable magnetic field [1–8]. The main distinguishing features of the VMV from the magnetometer described in [1–8] are the use of an optically pumped sensor [9, 10] and a continuous fast rotation of a transverse magnetic field. The same concept underlies the potassium magnetometer–variometer described in [11]. This study makes a step forward on the road to miniaturization of the device and an increase in its sensitivity. The idea is to place a fast quantum magnetometer at the center of a highly stable system of magnetic rings that is oriented relative to the geomagnetic field and produces a variable magnetic field the vector of which precesses about the geomagnetic field vector. The ring system is a combination of an adjusted solenoid with the axis directed along the geomagnetic field vector and two ring windings producing mutually orthogonal fields in the plane perpendicular to the geomagnetic field. The windings are excited by a sinusoidal current with frequency f (several tens or hundreds of hertz) so that the current phases in them are shifted by 90° relative to each other. As a result, the windings produce a field whose vector rotates with frequency f in the plane perpendicular to the geomagnetic field. A direct current passing through the solenoid induces a magnetic field compensating for ≈95% of the geomagnetic field. When all three currents are switched on simultaneously, the vector of a magnetic field formed at the center of the system precesses about the geomagnetic field with an apex angle from 30° to 60°.

The schematic of a VMV is shown in Fig. 1. The design of the sensor is standard: a spherical (or cylindrical) cell about 20 mm in diameter covered by a paraffin film from inside is filled with the cesium vapor. The nonuniformity of the field produced by the ring system does not exceed 1 nT within the cell. The cesium vapor is optically pumped at room temperature by the circularly polarized radiation of a cesium lamp. An interference filter separates out resonance line *D1* ($\lambda = 8943$ Å) from the pumping radiation. The pump beam is directed along the VMV axis (i.e., at an angle of 30°–60° to the magnetic field vector), thereby making the M_x signal observable. This signal is excited by applying a high-frequency current from a digital frequency synthesizer to the rf coil of the sensor. The synthesizer (synthesized frequency) is controlled by a microcontroller. The microcontroller, in turn, is controlled by an analog signal from the output of a phase detector, which tunes the synthesizer to the resonance frequency by using the phase dependence of the M_x signal. The M_x signal frequency depends on the absolute value of the rotating transverse field. The accuracy of the frequency depends on the remanent longitudinal magnetic field and the amplitude of the rotating transverse field. The magnetic resonance frequency remains constant when the exter-

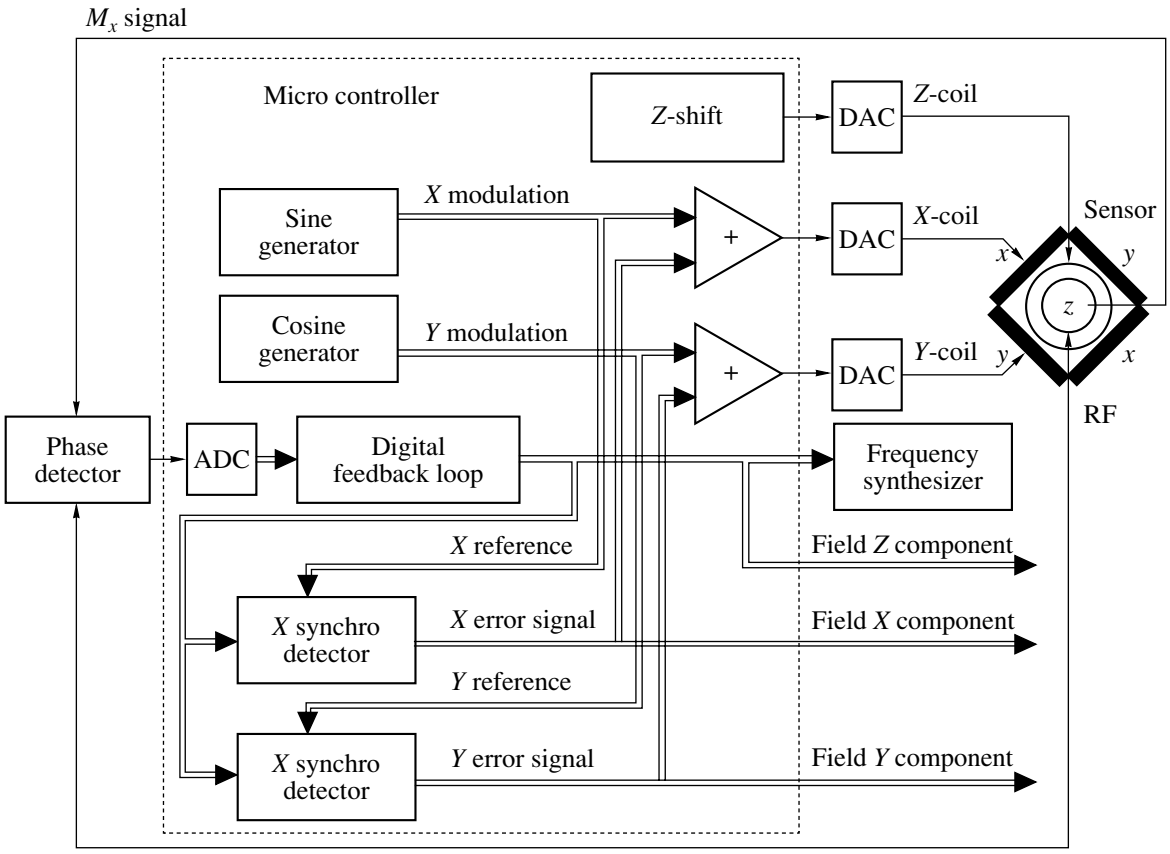

Fig. 1. Schematic of the vector magnetometer–variometer.

nal field is perfectly stable and the ring system axis is perfectly aligned with the field.

When the geomagnetic field transverse components change, the precession axis of the net magnetic field vector at the center of the system is deflected from the geomagnetic field vector. This leads (as will be shown below) to the modulation of the field magnitude in frequency f. A digital feedback system tracking the resonance frequency directly detects this modulation as the time dependence of the frequency synthesized. Two phase-orthogonal synchronous detectors operating at modulation frequency f were implemented in software. Their output signals, which vary in proportion to the geomagnetic field transverse components, are used to produce fields that completely compensate for these transverse components. The direct currents in the windings thus become a measure of variation of the geomagnetic field transverse components. The longitudinal component of the compensated geomagnetic field can be found from the magnitude of the resultant field vector and the rotating component amplitude, which are, respectively, the hypotenuse and leg of a right triangle. The transverse components are set (and measured) with a digital code used to program precision sources of current for the windings.

A more than tenfold decrease in the absolute value of the external permanent field (cf. [11]) allows one to appreciably increase the angle between the rotating magnetic vector and the axis of rotation (at the same magnitude of the latter) and, thus, to raise the detectability of the device in terms of geomagnetic field transverse components. Accordingly, the sizes of the sensor and ring system may be reduced by several times.

Cesium is an appropriate filler because of a high hyperfine splitting of its ground state and, accordingly, a small quadratic splitting of magnetic lines into sublevels. In magnetic field H, the resonance band appears as a set of equidistant lines spaced at 26.6 Hz $\times H^2$, where H is measured in oersteds. In an applied magnetic field of 0.07 Oe, the spacing is about 0.13 Hz, which is much smaller than the width of each of the lines. Thus, the lines actually constitute an intense and nearly symmetric band of magnetic resonance. This ensures a low systematic error in measuring the field longitudinal component.

The measured transverse components are free from systematic errors related to the sensor. Systematic errors may arise only from the instability of the electronic elements and faults in manufacturing the ring system. The use of a compensating magnetic field comparable in magnitude to a field being measured imposes

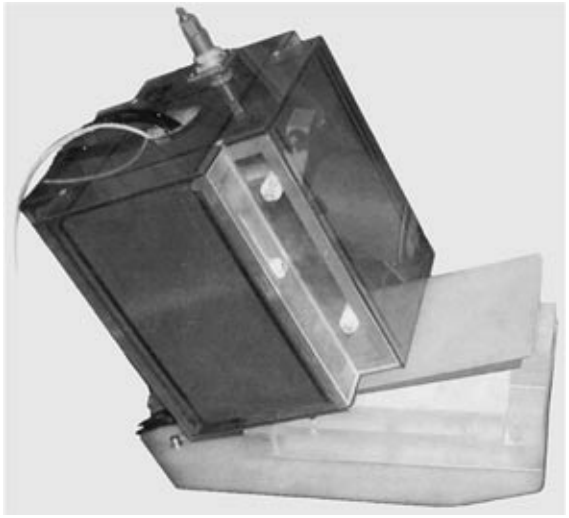

Fig. 2. Exterior view of the sensor of the variometer.

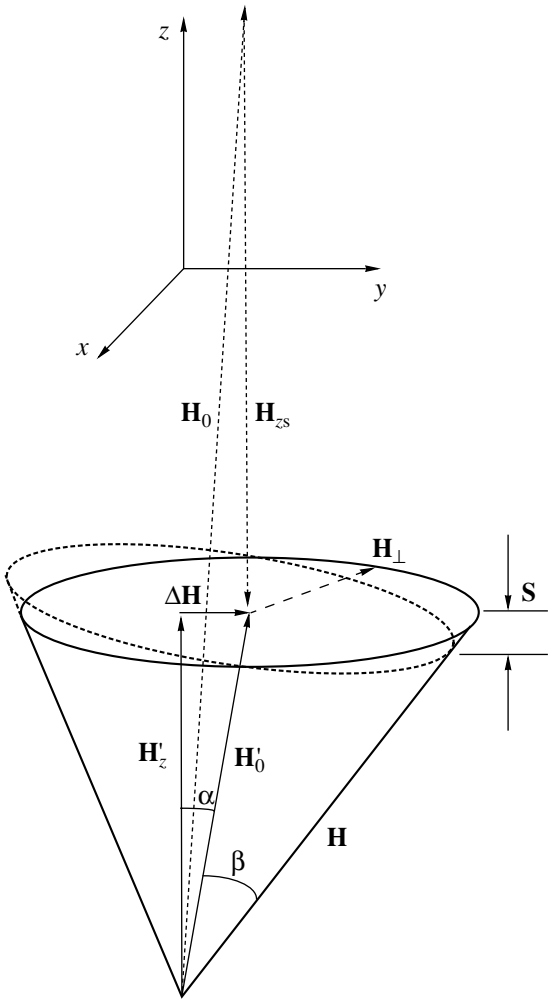

Fig. 3. Vector diagram illustrating the operation of the device.

much more stringent stability standards: the instability both of the ring system (solenoid) and of the current sources producing the compensating and rotating magnetic fields must be within 0.1 nT. To meet this requirement, the framework of the ring system was made of fused quartz and tailor-made microprocessor-controlled current sources with a relative instability of 5×10^{-6} were integrated into the general VMV circuit. The incorporation of a 32-bit frequency synthesizer controlled by a microprocessor with 8-bit analog inputs into the feedback loop made it possible to minimize the frequency noise in the x–y channels and, at the same time, to measure the frequency with an accuracy of 10^{-8} for 0.1 s. Also, microprocessor control allowed us to cut the processing time of the magnetic field deflection signal to one period of the external field and to suppress signal components at the second harmonic of the modulation frequency (which typically arise in analog processing). Finally, microprocessor control of the electronics necessitated the development of a convenient and ergonomic MS Windows-based device control and data acquisition/processing programmable interface.

Structurally, the variometer consists of a sensor and a ring system that are integrated into a $23 \times 23 \times 23$-cm case mounted on a tilted quartz support (Fig. 2), as well as of a pumping lamp and an electronic unit that are positioned at a distance of 2–3 m from each other and connected with the sensor by optical fibers and coaxial cables. The quartz support is equipped with mechanical positioners for precise alignment of the axis. The electronic unit is connected to a computer (the termination of the device) by a cable 50 m long. The terminating computer exchanges data with the system via a serial RS-232 cable and controls the device with instructions in the ASCII-format.

2. OPERATION OF THE DEVICE

The vector diagram in Fig. 3 illustrates the formation of a magnetic field at the center of the sensor. Initially, the z axis is aligned with geomagnetic field $\mathbf{H}_0$ (in Fig. 3, field $\mathbf{H}_0$ deviates from the initial direction by small angle α). Field $\mathbf{H}_{zs}$ generated by the solenoid to a large degree compensates the z component of field $\mathbf{H}_0$, and $\mathbf{H}'_0 = \mathbf{H}_0 + \mathbf{H}_{zs}$ is the sum of these two vectors. The orthogonal coils produce magnetic field $\mathbf{H}'_0$ rotating in the plane (x, y) with frequency f so that, at $\mathbf{H}_0 \parallel z$, the resultant field at the center of the sensor, $H = |\mathbf{H}| = (H_0^2 + H_\perp^2)^{1/2}$, does not contain harmonics at the rotation frequency. The situation changes when the field vector deflects from the z axis: amplitude $|\mathbf{H}|$ of the field now contains a component oscillating with frequency f, and the amplitude, S, and phase, φ, of these components depend, respectively, on the magnitude and direction of geomagnetic field transverse component $\Delta\mathbf{H}$.

As is seen from Fig. 3, at $\Delta H \ll H_0'$, signal amplitude S can be expressed in the form

$$S = k\Delta H, \quad (1)$$

where

$$k = H_\perp/(H_0'^2 + H_\perp^2)^{1/2} = \sin\beta \quad (2)$$

is the factor of conversion of a change in the field transverse component to a signal at frequency f. Therefore, k grows with amplitude $H_\perp$ of the rotating field; however, an exceedingly high increase in $H_\perp$ may substantially reduce both the stability and sensitivity of measuring the z component. An alternative way is to decrease field $H_0' \approx H_0 - H_{zs}$ (H_0 and H_{zs} are oppositely directed). The minimum and maximum values of total field intensity H in the sensor are limited by geomagnetic field fluctuations ($\Delta H \ll H_0'$) and by the quadratic splitting of the cesium line, respectively.

The sensitivity of the sensor attains maximum at $\beta = 45°$; however, the initial value of β was taken so as to maximize the sensitivity in an as wide a range of the geomagnetic field z component as possible rather than at one point.

Finally, we take $H_\perp$ in the range from 1.5 to 3 μT and $\beta = 40°$. Substituting this value of β into (2) yields $k = 0.63$. Therefore, the sensitivity of measuring the transverse components is expected to be lower than the sensitivity of measuring the field magnitude by a factor of $1/k \approx 1.6$.

Strictly speaking, when calculating the sensitivity for the transverse components, one should also take into account the efficiency of synchronous detection of the error signal at rotation frequency f, which also includes geomagnetic field fluctuations at frequency f. The spectrum of such fluctuations was analyzed in [11].

The decrease in the field intensities and the use of a cesium cell made it possible to considerably diminish the ring system dimensions compared with [11]. This, however, may adversely affect the long-term stability of measuring the z component of the field (H_z). In the measuring scheme presented in [11], the error in H_z was entirely defined by the instability of the field in the transverse coils, which was low because of the smallness of angle β ($\beta = 5.6°$). In the scheme used in this study, H_z is calculated from the measured value of field H in the sensor and known values of fields H_{zs} and $H_\perp$ (in the absence of uncompensated transverse components, $H_z = H_0$),

$$H_z = H_{zs} + (H^2 - H_\perp^2)^{1/2}; \quad (3)$$

accordingly, $|dH_z/dH_{zs}'| = 1$ and $|dH_z/dH_\perp| = \tan\beta = 0.82$. In other words, if field variations in the x, y, and z coils are equal to each other, the associated conversion coefficients and the errors in measuring the z component are nearly the same. Since the absolute value of the field in the solenoid, H_{zs}, is 20 times the values in the x and y coils ($H_\perp$), the long-term stability of the device is totally defined by the stability of the field in the z coil.

It its turn, the stability of the field in the solenoid depends mainly on the stability of the ring system parameters and the stability of the current sources feeding the ring system. The former is attained by using a framework made of fused quartz with a thermal expansion coefficient of 6×10^{-6} 1/°C; the latter, by applying precision sources of reference voltage, digital-to-analog converters (DACs), highly stable voltage followers, and superstable measuring resistors. The total temperature instability is estimated as 6×10^{-6} 1/°C. The long-term stability is associated with the aging of the Vishay precision current-measuring resistors (~10^{-4}). The problem of stability of analog electronic components it is expected to be solved by periodic automatic calibration of the system at the magnetic resonance frequency in a sufficiently stable magnetic field.

3. EXPERIMENT

The VMV was tested using both a magnetic shield and a magnetic field regulator.

The characteristics analyzed in this work were the following: (i) the signal amplitude, the angular range of capture, and the variation sensitivity as functions of the precession angle (the angle between the rotating field and the axis (Fig. 4); (ii) the angular range of capture and the variation sensitivity as functions of the modulation frequency (Fig. 5); (iii) the frequency response; (iv) the speed of the device, i.e., the response to a harmonic variation of the growing field; (v) the variation sensitivity as applied to the x, y, and z components (Fig. 7); (vi) and the reproducibility of the results.

The test results indicate that, when the parameters are adjusted to a maximal variation sensitivity, the geomagnetic field transverse components providing the capture of the magnetic resonance signal do not exceed ±100 nT. This limitation has a clear physical explanation. Indeed, in the presence of a rotating magnetic field, a deflection of the rotation axis from the geomagnetic field direction results in the modulation of the field amplitude at the rotation frequency (the basic principle of a variometer). In spectral terms, such a periodic modulation gives rise to signal components that are offset from the initial component by multiples of the modulation frequency. The amplitudes of these components are described by the Bessel functions. At low modulation frequencies, the amplitudes of the lateral harmonics become equal to the amplitude of the fundamental harmonic and so the capture of a desired frequency turns out to be virtually impossible. However, if a desired harmonic is still captured, the feedbacks in transverse components are activated, which bring the rotation axis into coincidence with the direction of the permanent field (the angle between them becomes

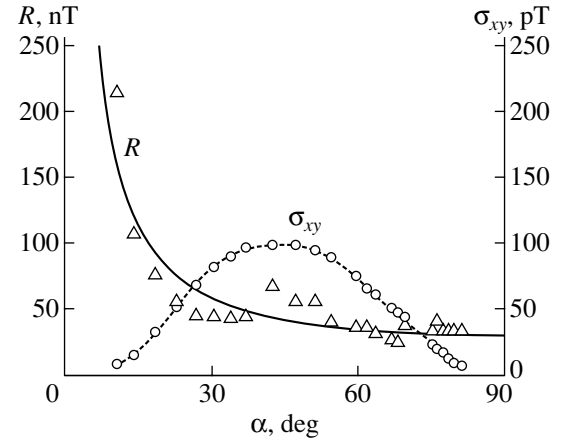

Fig. 4. (△) Angular range of capture R and (○) x–y sensitivity σ_{xy} vs. precession angle α. The solid line shows the theoretical σ_{xy} vs. α dependence.

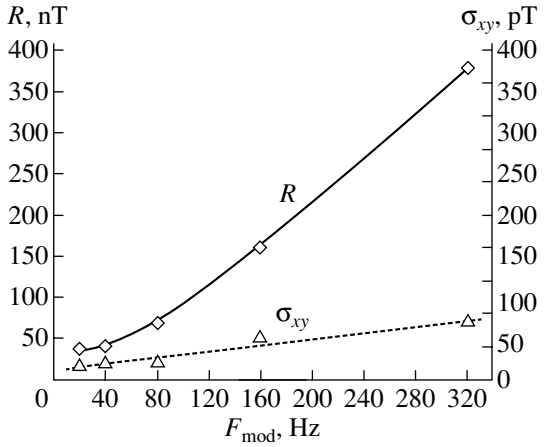

Fig. 5. (◇) Range of capture R and (△) x–y variation sensitivity σ_{xy} vs. transverse field rotation frequency.

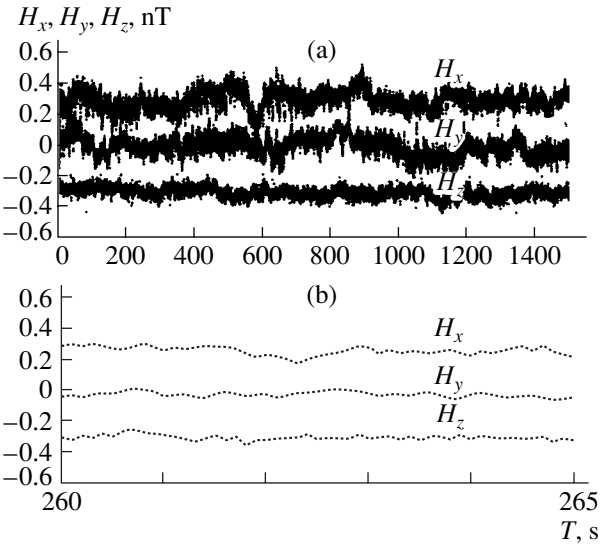

Fig. 6. (a) Summary records of the geomagnetic field variations under the active stabilization of the respective field components by the remote sensor and (b) a 5-s fragment of the same records.

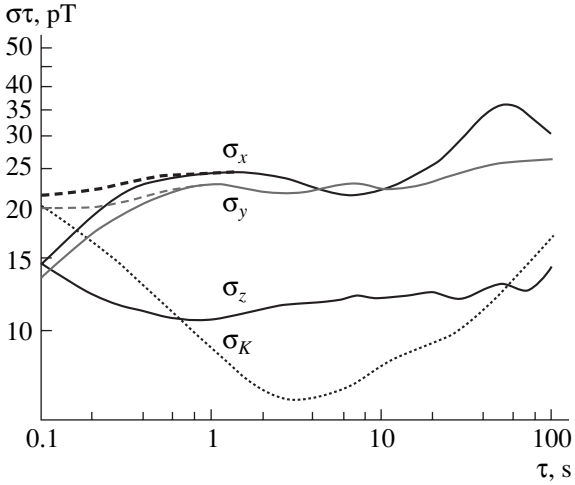

Fig. 7. Summary Allan diagram for the records in Fig. 6 made under the same conditions. The dashed curves correspond to the values of σ_x and σ_y with regard to time constant τ_{xy} = 0.11 s of the system; the dotted line (σ_K) shows the geomagnetic field variations measured by a potassium M_x magnetometer.

equal to zero) and, thus, provide the operation of the device under the conditions of the "pure" spectrum.

The initial range of capture was extended by complicating the capture algorithm. First, the magnetic resonance signal is sought with the parameters adjusted to a maximal range of capture (rotation frequency f = 640 Hz and angle of deflection $\beta = 22°$). After the resonance has been captured, parameters H_{zs}, f, and β are smoothly varied. As a result, the range of reliable capture was extended to ±750 nT.

The frequency response of the device showed that effective time constant τ in the channels of the transverse, x and y, components varies from 0.03 to 1 s depending on the amplification factor in the feedback loop. In subsequent experiments, the parameters were taken such that τ fell into the range between 0.1 and 0.15 s. The variations of the x and y components were detected at a rate of 780 nT/s.

Figure 6 presents the summary records of the geomagnetic field variations under active stabilization of all three components (each component was recorded separately). The associated Allan diagrams are shown in Fig. 7. The suppressed noise in the x and y channels at short times is due to a small time constant of the system, τ_{xy} = 0.11 s. The dashed portions show the variations "recovered" with due regard to τ_{xy}.

The main conclusion following from Figs. 6 and 7 is a good fit of the variations to ratio $\sigma_{xy}/\sigma_z = 1/k$. Indeed, it follows from Fig. 7 that $\sigma_{xy}/\sigma_z = (1.8 \pm 0.4)$, which agrees with formula (2) yielding $1/k = 1.6$. It should be noted that, in our experiment, σ_z depends largely on residual instabilities of the magnetic field in the regulator, which is spaced 20 m from the sensor, rather than on the intrinsic sensitivity of the cesium sensor. Therefore, the measured values of $\sigma_{xy} = \sigma_z/k$ are also overestimated. Yet, the upper estimate of the noise can be made. To do this, the geomagnetic field variations in the regulator were measured by a potassium scalar sensor (Fig. 7, dotted line). For a measurement time of 0.1 s, the VMV noise (a standard deviation of 0.022 nT) is almost indiscernible against the background of the intrinsic variations of the magnetic field in the regulator (a standard deviation of 0.020 nT). Hence, it follows that the standard deviation of the VMV intrinsic noise is within 0.010 nT for a measurement time of 0.1 s.

We also analyzed the start-to-start reproducibility of indications in the z channel of the VMV: the deviation remained within ±0.15 nT. Admittedly, the long-term stability (especially of the z channel) was not investigated to the full extent. To reach a stability within ±0.1 nT in the z channel requires further exploration and minimization of drifts. All the measurements were carried out indoors with the ambient temperature kept at $T = (22 \pm 2)$°C.

We developed and tested a procedure of automatic calibration of the constants of the x, y, and z coils, as well as of their cross-constants, with the aim to avoid the nonorthogonality of the coil axes and misarrangement of the sensor in the ring system. The calibration procedure is accomplished in a stabilized or undisturbed field and requires no additional equipment. The accuracy of automatic calibration, δH, depends on sensitivity σ_z, external magnetic field instability ΔH_0, field variation ΔH_i ($i = x, y, z$) in the coil tested, total working field H_i, in the coil, and number of tests N; that is,

$$\Delta H = (1/k)(1/N)^{1/2}(\sigma_z^2 + \Delta H_0^2)^{1/2}(H_i/\Delta H_i), \quad (4)$$

where $H_x/\Delta H_x = H_y/\Delta H_y = 2$ and $H_z/\Delta H_z \approx 1.5$.

Therefore, to calibrate the z coil with an accuracy of ~0.1 nT in a field stabilized to $\Delta H_0^2 \le \sigma_z^2$, it suffices to repeat the calibration procedure four to six times.

Currently, a more compact ring system with higher order rings is under development. A compact ring system would provide temperature control throughout the VMV volume and ring system and, thereby, to lower drifts in the z channel by one to two orders of magnitude.

CONCLUSIONS

The vector magnetometer–variometer presented here can be used as an absolute instrument for geophysical observatories. A combination of long-term stability and high speed, which is lacking in quantum precession magnetometers, sets off this VMV from other devices serving similar purposes.

ACKNOWLEDGMENTS

We thank V.Ya. Shifrin and E.N. Choporova for the opportunity for experimentation at the magnetic station at the Institute of Metrology.

REFERENCES

1. P. Jung and J. van Cakenbergne, Arch. Sci. (Geneva) **14**, 132 (1961).
2. L. R. Alldredge and I. Saldukas, *The Automatic Standard Magnetic Observatory: US Technical Bulletin No. 31*, Department of Commerce, Environmental Science Services Administration, Coast and Geodetic Survey (GPO, Washington, 1966).
3. A. P. De Vuyst, *Report to the General Assembly of the International Association of Geomagnetism and Astronomy, Moscow, 1971.*
4. A. J. Fairweather and M. J. Usher, J. Phys. E **5**, 986 (1972).
5. M. J. Usher and J. P. Reid, J. Phys. E **11**, 1169 (1978).
6. J. L. Rasson, Geophys. Trans. **36**, 187 (1991).
7. A. Khokhlov, O. Gravrand, J.-L. Le Mouél, and J. M. Leger, Earth, Planets, Space **53**, 949 (2001).
8. J. J. Schott, A. Pérès, and J. M. Cantin, in *Proceedings of the 10th IAGA Workshop on Geomagnetic Instruments Data Acquisition and Processing, Hermanus, 2002*, p. 147.
9. E. B. Alexandrov, M. V. Balabas, A. K. Vershovskii, *et al.*, Opt. Spektrosk. **78**, 325 (1995) [Opt. Spectrosc. **78**, 292 (1995)].
10. E. B. Alexandrov, M. V. Balabas, A. K. Vershovskii, *et al.*, in *Proceedings of the International Conference on Marine Electromagnetic (MARELEC-97), London, 1997*, p. 8.
11. E. B. Alexandrov, M. V. Balabas, V. N. Kulyasov, *et al.*, Meas. Sci. Technol. **15**, 918 (2004).

Translated by A. Sidorova